energies

MDPI

Article

Fe^{I} Intermediates in N_2O_2 Schiff Base Complexes: Effect of Electronic Character of the Ligand and of the Proton Donor on the Reactivity with Carbon Dioxide

Ruggero Bonetto *, Daniel Civettini, Francesco Crisanti and Andrea Sartorel *

Department of Chemical Sciences, University of Padova, Via Marzolo 1, 35131 Padova, Italy; daniel.civettini@studenti.unipd.it (D.C.); francesco.crisanti@studenti.unipd.it (F.C.)

* Correspondence: ruggero.bonetto@studenti.unipd.it (R.B.); andrea.sartorel@unipd.it (A.S.); Tel.: +39-049-8275667 (R.B.); +39-049-8275252 (A.S.)

Abstract: The characterization of competent intermediates of metal complexes, involved in catalytic transformations for the activation of small molecules, is an important target for mechanistic comprehension and catalyst design. Iron complexes deserve particular attention, due to the rich chemistry of iron that allows their application both in oxidation and reduction processes. In particular, iron complexes with tetradentate Schiff base ligands show the possibility to electrochemically generate Fe^{I} intermediates, capable of reacting with carbon dioxide. In this work, we investigate the electronic and spectroscopic features of Fe^{I} intermediates in five Fe(L_{N2O2}) complexes, and evaluate the electrocatalytic reduction of CO_2 in the presence of phenol (PhOH) or trifluoroethanol (TFE) as proton donors. The main findings include: (i) a correlation of the potentials of the $Fe^{II/I}$ couples with the electronic character of the L_{N2O2} ligand and the energy of the metal-to-ligand charge transfer absorption of Fe^{I} species (determined by spectroelectrochemistry, SEC-UV/Vis); (ii) the reactivity of Fe^{I} species with CO_2, as proven by cyclic voltammetry and SEC-UV/Vis; (iii) the identification of Fe(salen) as a competent homogeneous electrocatalyst for CO_2 reduction to CO, in the presence of phenol or trifluoroethanol proton donors (an overpotential of 0.91 V, a catalytic rate constant estimated at 5×10^4 s^{-1}, and a turnover number of 4); and (iv) the identification of sudden, ligand-assisted decomposition routes for complexes bearing a ketylacetoneimine pendant, likely associated with the protonation under cathodic conditions of the ligands.

Keywords: Iron N_2O_2 Schiff base complexes; Fe^{I} intermediates; CO_2 reduction; spectroelectrochemistry

Citation: Bonetto, R.; Civettini, D.; Crisanti, F.; Sartorel, A. Fe^{I} Intermediates in N_2O_2 Schiff Base Complexes: Effect of Electronic Character of the Ligand and of the Proton Donor on the Reactivity with Carbon Dioxide. *Energies* **2021**, *14*, 5723. https://doi.org/10.3390/en14185723

Academic Editor: Julien Warnan

Received: 29 July 2021
Accepted: 7 September 2021
Published: 11 September 2021

1. Introduction

Iron coordination compounds are intensively investigated for driving several chemical transformations, in particular involving oxidation/reduction processes. A key feature is the ample redox chemistry of the iron metal center that enables the formation of either high-valent Fe^{IV} or Fe^{V} oxo intermediates [1,2] or low-valent Fe^{I} or Fe^{0} derivatives [3–7] involved in the reductive transformation of protons, nitrogen, and carbon dioxide. Focusing in particular on CO_2, the nature of the low-valent iron intermediate, together with the combination of suitable additives, have been shown to impact the selectivity of the process, with possible products being carbon monoxide, formate, or highly reduced methanol and methane [8].

Iron porphyrins, where iron is coordinated by a N_4 tetradentate *heme* motif, are the most investigated class of coordination compounds for the reduction of CO_2, and operate through the generation of a formal Fe^{0} state that binds CO_2 and further promotes its conversion [9]. Conversely, iron complexes with tetradentate N_2O_2 Schiff base ligands have been less explored; examples have reported the use of 2-hydroxybenzene pendants on 1,10-phenanthroline (2,9-bis(2-hydroxyphenyl)-1,10-phenanthroline, dophen) [10], 2,2′-bipyridine scaffolds (6,6′-di(3,5-di-tert-butyl-2-hydroxybenzene)-2,2′-bipyridine, $^{t\mathrm{Bu}}$dhbpy) [11],

and a recent report by some of us taking advantage of the N,N′-bis(salicylaldehyde)-1,2-phenylenediamine (salophen) ligand [12]. In Fe(salophen), the reactivity with CO_2 involves an electrogenerated Fe^I intermediate, that in the presence of phenol as the proton donor, leads to the selective production of CO with appealing catalytic properties including an overpotential of 0.65 V and a turnover frequency up to 10^3 s^{-1} [12]; the nature and the concentration of the proton donor were found to play a key role in the catalytic process, in terms of product selectivity and of Fe(salophen) stability [12]. These findings, together with the ease of preparation of these complexes in gram scale, prompted us to investigate the reactivity of other Fe complexes with N_2O_2 ligands, focusing in particular on the characterization of the Fe^I intermediate and on its reactivity. Comprehension and rationalization of the reactivity of Fe complexes with N_2O_2 ligands are indeed important for catalyst design, aimed at the development of efficient CO_2 conversion.

In this work, we consider four iron complexes with tetradentate N_2O_2 Schiff base ligands, bearing an additional chlorido ligand, $Fe^{III}Cl(L_{N2O2})$, where L_{N2O2} is readily prepared by condensating ethylenediamine with salicylaldehyde, acetylacetone, or benzoylacetone. We will show that these complexes undergo two stepwise metal-centered reductions, leading to the formation of Fe^I intermediates. Reduction potentials of the $Fe^{II/I}$ couples correlate with the DFT calculated electronic character of the L_{N2O2} and with spectroscopic features of the Fe^I intermediate. Fe^I species react with CO_2, and the nature of the proton donor additive is crucial in promoting the transformation into CO with respect to competitive H_2 evolution.

2. Materials and Methods

Synthetic procedures were accomplished by adapting literature procedures.

Cyclic voltammetry experiments were conducted with a three-electrode system controlled by a BASi EC Epsilon potentiostat-galvanostat. The working electrode was a glassy carbon disk electrode (BioLogic, nominal diameter 3 mm), the auxiliary electrode was a platinum electrode (BASi), and the reference electrode was an Ag/AgCl/NaCl (3 M) electrode; potentials were then referenced to the ferrocinium/ferrocene (Fc^+/Fc) couple upon addition, at the end of each experiment session, of ferrocene to the analyte solutions as internal standard. 0.1 M tetraethylammonium tetrafluoroborate (Et_4NBF_4) was used as a supporting electrolyte.

Constant potential electrolysis experiments were performed with a Metrohm Autolab PGSTAT204 potentiostat-galvanostat controlled by Nova 2.1.4 software. The cell generally employed for preparative electrolysis was a custom-made, 6-necked, 2-compartment glass cell, with the two compartments being separated by a porous glass frit.

Gaseous product analysis was performed by gaschromatography equipped with a thermoconductimetric detector and a mass spectrometer. Gas samples of known volume were withdrawn from the headspace of the electrolysis cell by means of a gastight Hamilton syringe. Quantification of the gaseous species was achieved by external calibration of the instrument, upon the construction of a calibration curve by the injection of known volumes of pure gas.

^{1}H-NMR analysis for formate detection followed the protocol reported by Machan et al., by treating 2 mL of the electrolysis solution with 2 mL of D_2O, followed by washing twice with dichloromethane (formate is extracted in the D_2O phase) [11].

UV/Visible absorption spectroelectrochemistry (SEC-UV/Vis) experiments were performed by employing a Varian Cary 50 Bio spectrophotometer, equipped with a 0.5 mm nominal optical path quartz spectroelectrochemistry cell (BASi EF-1362). The electrodes used were a platinum gauze working electrode, a platinum wire auxiliary electrode, and an Ag/AgCl/NaCl (3 M) reference electrode. The reference and auxiliary electrodes were immersed above the thin layer of solution electrolyzed by the working electrode.

DFT calculations were performed at the B3LYP/6–311+g(d,p) level of theory, with Gaussian16 software.

Further details are reported in Supplementary Information.

3. Results

3.1. Fe Complexes with Tetradentate N_2O_2 Ligands

The ligands employed in this work and the corresponding iron(III) coordination complexes, bearing an additional chlorido ligand (Figure 1), were prepared by adapting literature procedures [12–14]. The identity and purity of the synthesized compounds were confirmed by ^{1}H and ^{13}C-NMR (only for the ligands), and by electrospray ionization mass spectrometry (ESI-MS), elemental analysis, and UV/Vis spectrophotometry (see Supplementary Information).

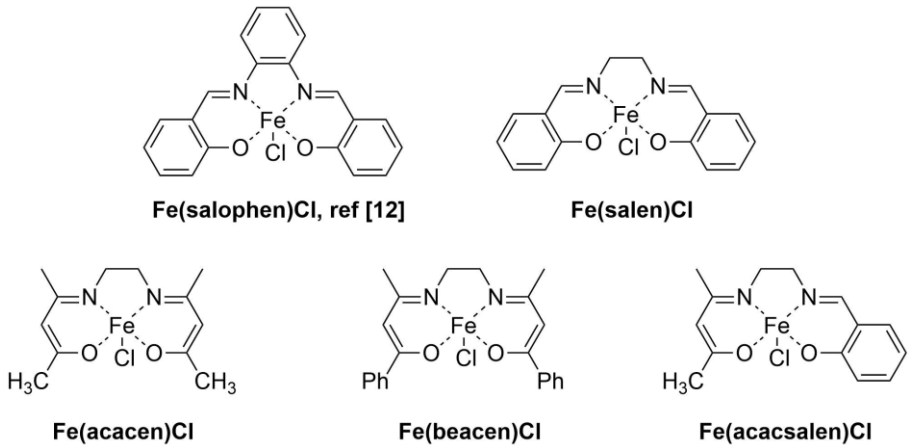

Figure 1. Iron complexes with tetradentate N_2O_2 ligands employed in this work. H_2salophen: N,N′-bis(salicylaldehyde)-1,2-phenylenediamine; H_2salen: N,N′-bis(salicylaldehyde)-1,2-ethylenediamine; H_2acacen: N,N′-ethylene-bis(acetylacetoneimine); H_2beacen: N,N′-ethylene-bis(benzoylacetoneimine); H_2acacsalen: N,N′-ethylene-(acetylacetoneimine)(salicylideneimine).

The ligands employed in this work and the corresponding iron(III) coordination complexes, bearing an additional chlorido ligand (Figure 1), were prepared by adapting literature procedures [12–14]. The identity and purity of the synthesized compounds were confirmed by ^{1}H and ^{13}C-NMR (only for the ligands), and by electrospray ionization mass spectrometry (ESI-MS), elemental analysis, and UV/Vis spectrophotometry (see Supplementary Information).

In Fe(salen)Cl, iron is pentacoordinated and shows an asymmetric structure closer to a trigonal bipyramid with respect to a square pyramid, according to the τ geometric parameter [15,16]. Concerning N,N′-ehtylenebis(ketylacetonylideneimine) Iron(III) complexes, the N_2O_2 chelating group is almost planar, while the chlorido ligand occupies an axial position, in a distorted square planar coordination geometry [11,17]. In all cases, in the absence of additional high field ligands [17], Iron(III) is expected to have a d^5 high spin (S = 5/2) configuration [11,17], and the complexes display ligand to metal charge transfer (LMCT) bands in the visible region (see Supplementary Information) [16]; absorptions in the UV region are due to intraligand charge-transfer transitions [18].

3.2. Electrochemical Properties and Spectroscopic Features of Fe^I Species

The electrochemical properties of Iron complexes were investigated by cyclic voltammetry (CV) in acetonitrile solutions, and are summarized in Table 1; Figure 2 (black traces under N_2) reports the CV traces of Fe(salen)Cl and of Fe(beacen)Cl as representative cases, while other CV traces are reported in Supplementary Information (Figure S1). Although the redox-active nature of Schiff base ligands is well-established [19–21], common electrochemical features under a cathodic scan encompassing these coordination compounds are two one-electron waves, due to stepwise reduction processes of the iron center and attributed to $Fe^{III/II}$ and $Fe^{II/I}$ couples, in which chlorido ligand binding equilibria are coupled to the electrochemical process driven by the working electrode potential (Figure 3) [11,12,22].

Table 1. Electrochemical and spectroscopic characterization of iron complexes employed in this work.

Iron Complex	$E_{1/2}$ (V) vs. Fc^+/Fc, V (ΔE, mV)		λ_{MAX} Fe^I [a]	$-i_{CO2}/i_{N2}$ [b]
	$Fe^{III/II}$	$Fe^{II/I}$		
Fe(salophen)Cl [12]	−0.69 (84)	−2.00 [c]	405	−2.1
Fe(salen)Cl	−0.77 (98)	−2.21 (89)	354	−4.2
Fe(acacen)Cl	−0.93 (93)	−2.50 (68)	288	−5.6
Fe(beacen)Cl	−0.83 (81)	−2.24 (93)	344	−5.3
Fe(acacsalen)Cl	−0.83 (91)	−2.25 (131)	308, 379	−4.1

[a] From SEC-UV/Vis analysis. [b] Determined from the ratio of the peak current in the scan with CO_2 and the peak current of the $Fe^{II/I}$ couple under dinitrogen; while being a useful parameter to evaluate the catalytic activity, the $-i_{CO2}/i_{N2}$ ratio is dependent on the scan rate; values in this table refer to scan rate = 0.1 V s^{-1}. [c] Quasi-reversible wave, and anodic backward peak only detectable at high scan rates (16 Vs^{-1}).

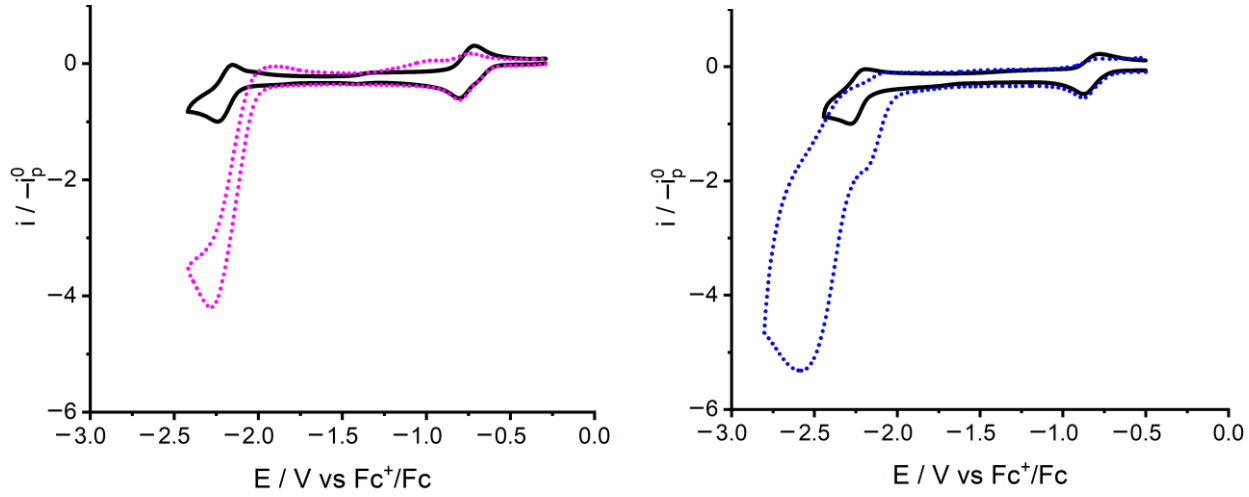

Figure 2. Cyclic voltammetries of 1 mM Fe(salen)Cl (**left**) and Fe(beacen)Cl (**right**) in acetonitrile (0.1 M Et_4NBF_4 electrolyte), under N_2 (black, solid traces) and CO_2 (dotted traces) atmosphere. The current of the voltammetries is normalized with respect to the peak current of the $Fe^{II} \rightarrow Fe^I$ reduction wave under dinitrogen, to visualize the enhancement in the presence of CO_2. The glassy carbon (GC) disk working electrode, Pt counter electrode, and Ag/AgCl/NaCl (3 M) were the reference electrode; potentials were then converted to Fc^+/Fc by internal calibration; scan rate 0.1 Vs^{-1}.

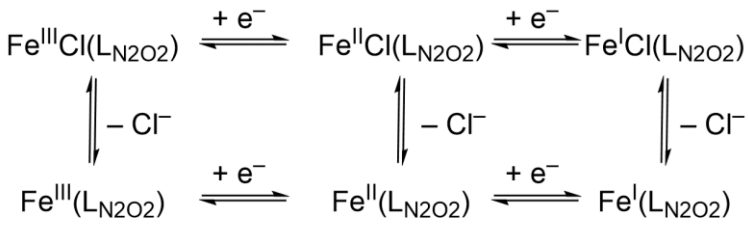

Figure 3. Redox equilibria of iron complexes. As previously observed for Fe (salophen)Cl [12], the loss of Cl^- should be considered relevant at the level of the Fe^I state under the conditions of the CV scans, in the absence of additional Cl^- sources.

The electrochemical behavior of the complexes at the level of their $Fe^{III/II}$ couples, first described by Carré et al. [23], is typical of a quasi-reversible transformation. Specifically, all $Fe^{III/II}$ waves display ΔE in the range 80–100 mV, as summarized in Table 1 and reported in the Supplementary Information (Figure S2), coherently with competition between the coordinating solvent and the chloride anion for the apical coordination site in the Fe^{III} and Fe^{II} states [11,12,22].

The second cathodic wave, encountered at more negative potentials, displays quasi-reversible features, depending on the Schiff base ligand coordinated to the iron ion. The

structural and electronic analogies justifying the group categorization of the iron complexes herein described are manifest in the accessibility of a low valent formal Fe^{I} state.

The electronic properties of the Schiff base ligands and their direct influence on the redox potentials of the $Fe^{III/II}$ and $Fe^{II/I}$ couples can be evaluated on the basis of the σ-donor strength of the N_2O_2 ligand [18,24]. Interestingly, in the series of the coordination complexes examined in this work, correlations are observed between the $Fe^{III/II}$ and $Fe^{II/I}$ reduction potentials and the energy of the highest occupied molecular orbital of the ligands (Figure S3) involved in σ-donation (HOMO-2), as predicted by DFT calculations at the B3LYP/6–311+g(d,p) level of theory: Slopes of -0.40 ± 0.04 and of -0.84 ± 0.11 V/eV are observed for the $Fe^{III/II}$ and $Fe^{II/I}$ couples, respectively (see Figures S4 and S5 in Supplementary Information). Notably, the almost double slope value observed for the $Fe^{II/I}$ couples with respect to the $Fe^{III/II}$ ones indicates a higher impact of the nature of the ligand on the reduction potentials of the former couple. This could be ascribed to the fact that the $Fe^{III} \rightarrow Fe^{II}$ transition is expected to be charge neutral upon loss of the Cl^{-} ligand, while the $Fe^{II} \rightarrow Fe^{I}$ transition is expected to generate a negative charge at the complex (Figure 3). The symmetry of the metal orbitals involved in the redox transformation is also important to support the observed changes in the redox properties caused by ligand electronic effects [18,25].

The formation of an Fe^{I} intermediate was previously corroborated by electron paramagnetic resonance (EPR) spectroscopy for Fe(salophen) [12]. Further confirmation of the electrochemical generation of the Fe^{I} species comes from spectroelectrochemistry in the UV/Vis region (SEC-UV/Vis). Figure 4 reports the absorption traces of Fe(salen)Cl and Fe(beacen)Cl as representative examples, while the other iron complexes are shown in Figure S6 in Supplementary Information. Upon application of the potentials associated with the second reduction waves (-2.21 and -2.24 V vs. Fc^{+}/Fc for Fe(salen) and Fe(beacen), respectively), consistent UV/Vis spectra changes are observed (Figure 4 top), and in particular: (i) Bleaching of the initial absorption of the Fe^{III} species (464 and 311 nm for Fe(salen)Cl and 492 and 293 nm for Fe(beacen)Cl), attributed to ligand-to-metal charge transfer bands, LMCT; and (ii) rising of new bands (344 nm for Fe(salen) and 354 nm for Fe(beacen)), attributed to metal-to-ligand charge transfer bands (MLCT) from the electron-rich Fe^{I} state.

Two further points are worthy of mention:

(i) In the case of the Fe(acacsalen)Cl, two absorption features rise upon generation of Fe^{I} at 308 and 379 nm, respectively (see Figure S6); these two MLCT components are expected on the basis of the peculiar character of the asymmetric acacsalen ligand, bearing both the acetylacetoneimine and salicylideneimine pendants. Incidentally, the two absorption maxima observed for Fe^{I}(acacsalen) are similar to those observed separately for Fe^{I}(acacen) (288 nm) and for Fe^{I}(salen) (354 nm).

(ii) The energy of the MLCT band observed for the Fe^{I} intermediates correlates linearly with the redox potential of the $Fe^{II/I}$ couple; the trend shows that the more negative the potential of the $Fe^{II/I}$ couple, the higher the energy of the MLCT band (absorption shifted towards the blue region of the spectrum, Figure S7).

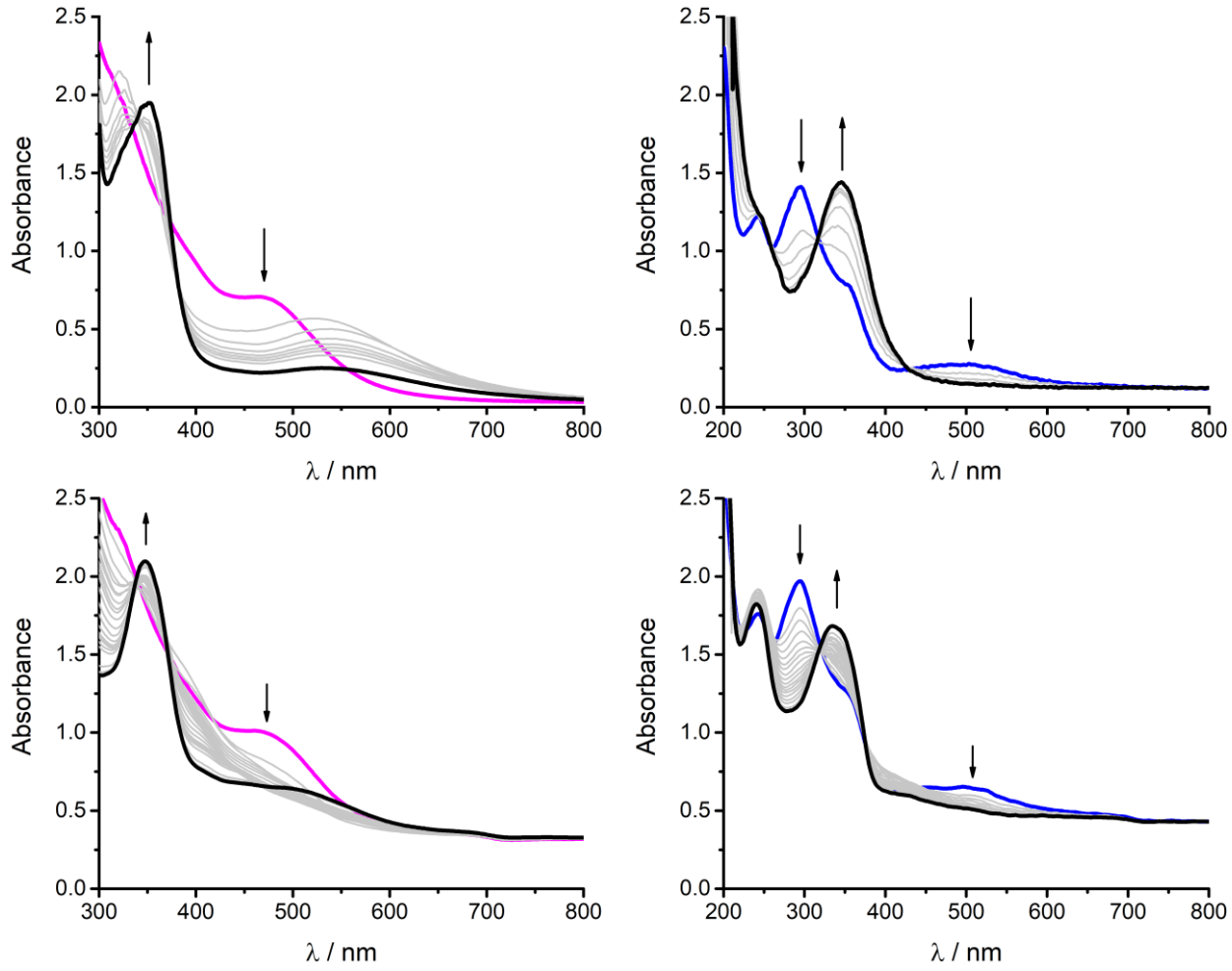

Figure 4. SEC-UV/Vis traces of Fe(salen)Cl (**left**) and of Fe(beacen)Cl (**right**) under N_2 atmosphere (**top panels**) and under CO_2 atmosphere (**bottom panels**), at the potentials corresponding to the generation of the formal Fe^I state (−2.21 and −2.24 V vs. Fc^+/Fc for Fe(salen) and Fe(beacen), respectively).

3.3. Reactivity of Fe^I towards Carbon Dioxide

In the presence of carbon dioxide, the voltammetric traces of the iron complexes display intense, irreversible peak-shaped waves at the level of the $Fe^{II/I}$ couple (see the i_{CO2}/i_{N2} parameter summarized in Table 1, where i_{CO2} is the peak current of the wave under CO_2, and i_{N2} is the peak current of the one-electron cathodic wave of the $Fe^{II/I}$ couple under dinitrogen atmosphere). The features of the wave observed under a CO_2 atmosphere are indicative of an electrocatalytic event involving the active Fe^I intermediate generated at the electrode, as evident in Figure 2 for Fe(salen)Cl and Fe(beacen)Cl as representative cases (see Figure S1 for the other complexes). In the case of Fe(beacen)Cl, the wave observed in the presence of CO_2, is composed of two contributions. A pre-wave, observed at −2.20 V vs. Fc^+/Fc (positively shifted by 80 mV with respect to the cathodic $Fe^{II/I}$ peak under N_2 atmosphere), is followed by the more intense wave peaking at E_p = −2.58 V vs. Fc^+/Fc. Such an observation is likely ascribable to two different reduction pathways—associated with different reduced intermediates—of which the second, generated at more cathodic potentials, is involved in a faster catalytic reaction [26]. The first cathodic wave observed in the presence of CO_2 could therefore be reasonably attributed to a slower process, proceeding through an adduct obtained as the irreversible association between CO_2 and the reduced Fe^I complex, as previously observed in the case of an iron quaterpyridine catalyst [5]. Attempts to estimate association parameters between Fe^I and CO_2 are hampered by the ill-defined nature of the pre-wave and the underlying current associated with the

catalytic process, occurring at potentials close to the first process. We anticipate that in the presence of proton donors (vide infra), the subsequent catalytic current will be enhanced at this potential, most likely due to a protonation-first pathway of the reduced adduct, promoting the catalytic transformation [27].

Reactivity of the Fe^{I} species with CO_2 was further supported by two complementary experiments:

(i) SEC-UV/Vis analysis in the presence of CO_2, where the diagnostic MLCT features of the Fe^{I} intermediate are blue-shifted with respect to those observed under dinitrogen (Figure 4 bottom). In particular, the absorption maximum shifts from 354 to 345 nm for Fe(salen) and from 344 nm to 332 nm for Fe(beacen); in the case of Fe(salophen), the MLCT shifted from 405 nm to 385 nm in the presence of CO_2 [12]. A spectroelectrochemical analysis in the infrared region (SEC-IR) failed to reveal absorption features ascribable to stretching features of iron-carbonyl intermediates, as was observed in the case of Fe(salophen), ref. [12]. This could be ascribed to an enhanced reactivity of such intermediates, although the interference of platinum working electrode at the negative operative in our setup should be also considered.

(ii) Isolation of Fe^{I} species upon constant potential electrolysis under inert atmosphere, followed by the addition of carbon dioxide (in the absence of applied potential), that led to an immediate color change of the solution (see pictures in Figure S8 in Supplementary Information). In the case of Fe(salophen), the reactivity of Fe^{I} with CO_2 under analogous conditions was associated with a redox process involving the oxidation of Fe^{I} to Fe^{III} by CO_2, as supported by EPR evidence [12]. Notably, no reduced products of CO_2 were detected under these conditions (in particular, carbon monoxide), suggesting that a further reduction of the $Fe^{I}-CO_2$ adduct is required in order to close the cycle and release the products (vide infra).

The electrocatalytic process impacts the behavior observed in the backward scan. Indeed, the anodic trace recorded in the presence of CO_2 displays an abatement of the $Fe^{II/III}$ oxidation wave. In the case of Fe(salen)Cl, a new anodic peak (E_p = −0.93 V vs. Fc^+/Fc) arises, 210 mV more negative than the $Fe^{II/III}$ oxidation peak (Figure 2). These observations are ascribable to chemically irreversible transformations of the complexes induced by the applied potential in the presence of CO_2 acting as a substrate. These processes might involve the loss or exchange of apical ligands in the coordination sphere of the iron ion, most likely involving CO [3,12,28,29]. Interestingly, a recovery of the reversibility of the $Fe^{III/II}$ couple in CV scans is observed in the presence of proton donors (see Section 3.4), which can facilitate the conversion of reduced intermediates and the regeneration of the parent form of the complex.

3.4. Effect of Proton Donors and Electrolysis

In order to evaluate and characterize the putative electrocatalytic reduction of CO_2 in the presence of the iron complexes, the use of a proton donor adjuvant should be considered [3,27–30]. Following the indication of a previous screening conducted with Fe(salophen), phenol (PhOH, pK_a = 29 in acetonitrile [29]) was considered, since it provided high selectivity for CO formation, also supported by $^{13}CO_2$ labelling experiments [12]. Trifluoroethanol was also evaluated (TFE, pK_a = 35.4 in acetonitrile [27,30], although a value of 25.1 was estimated in the presence of CO_2 due to the reaction of the trifluoroethoxide conjugate base with CO_2 to give the $CF_3CH_2OCO_2^-$ carbonate [30]) since it was recently used in combination with Mn-based CO_2 reduction catalysts [27]. The concentration of 0.3 M for TFE was selected as the one providing the maximum current in a CV screening with Fe(acacen)Cl.

The effect of the proton donors in the presence of CO_2 was first investigated by CV (see representative traces in Figure 5 for Fe(beacen)Cl and Fe(salen)Cl; the CV traces for the other complexes are reported in Figures S9–S11), by choosing 0.3 M and 0.5 M as the concentrations of TFE and PhOH, respectively [12]. The major effect is a further current increase of the cathodic wave at the level of the $Fe^{II/I}$ couple, as indicated by the

i_{CO2}/i_{N2} ratio (Table 2). This is coherent with a more efficient catalytic process, highlighting the beneficial role of mild proton donors in facilitating the further evolution of the putative Fe–CO_2 intermediate upon its stabilization by hydrogen bonding and stepwise protonation [27,28]. Notably, the presence of trifluoroethanol led to the observation of the $Fe^{II} \rightarrow Fe^{III}$ re-oxidation wave in the backward scans, likely indicative of a more efficient cycle, with a lower impact on the chemical stability of the catalytically active molecular species (vide supra).

Constant potential electrolysis (CPE) was then performed in order to identify and quantify the products associated with the cathodic waves, and to evaluate the stability of the systems. Three general considerations can be summarized as follows:

(i) Carbon monoxide (CO) and hydrogen (H_2) were the sole product identified; NMR analysis according to the procedure reported by Nichols et al. [11] did not reveal the production of formate (See Supplementary Information and Figure S14);

(ii) In all cases, the overall Faradaic yield of the process for CO and H_2 production is significantly lower than the ideal value; this is ascribed to both the need for pre-reducing the Fe^{III} to the active Fe^{I} state, and the consumption of reducing equivalents by the iron complexes leading to their inactivation and decomposition, as demonstrated by the drop of electrolysis current over time (Figure S15) and by the marked changes in the UV/Vis spectra after electrolysis (Figure S16). Non-quantitative Faradaic yields are not unusual in the electrochemical reduction of CO_2 with coordination complexes [5,12,31];

(iii) The use of phenol as the proton donor leads to a marked impact on the selectivity of the process depending on the iron complex. In particular, while high selectivity for CO is observed in the case of Fe(salophen) and Fe(Salen), H_2-oriented selectivity is observed for Fe(acacen), Fe(acacsalen), and Fe(beacen), as shown in Table 2 and Figure 6, i.e., for the species where the Fe^{I} intermediate is generated at more negative potentials and is thus expected to be more prone to a direct reaction with proton donors.

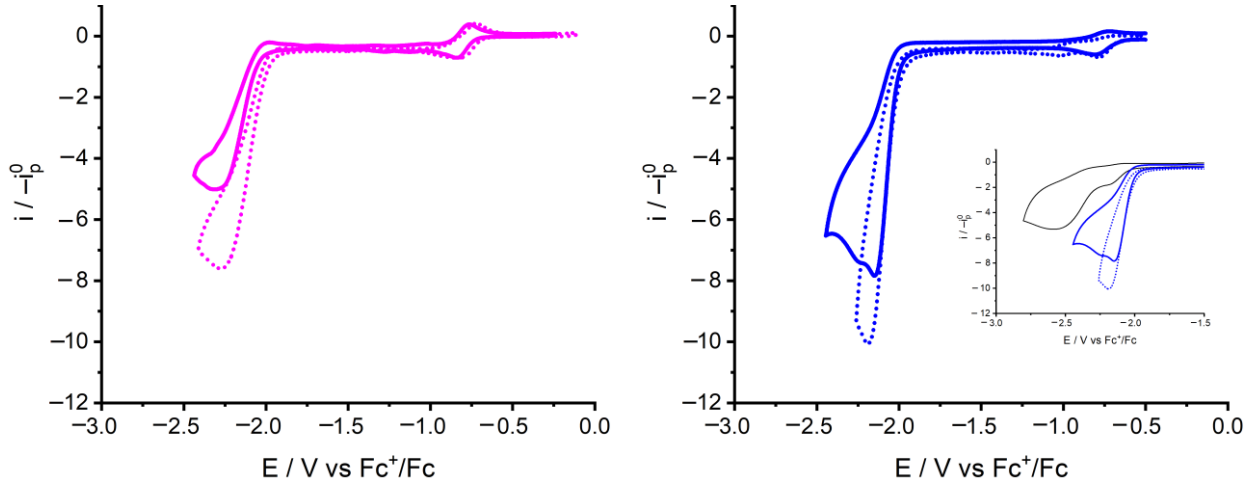

Figure 5. Cyclic voltammetries of 1 mM Fe(salen)Cl (**left**) and Fe(beacen)Cl (**right**) in acetonitrile (0.1 M Et_4NBF_4 electrolyte), under CO_2 atmosphere, in the presence of 0.3 M trifluoroethanol (TFE, solid traces) or 0.5 M phenol (PhOH, dotted traces) as proton donors. The current of the voltammetries is normalized with respect to the peak current of the $Fe^{II} \rightarrow Fe^{I}$ reduction wave under dinitrogen in the absence of proton donors, in order to allow a direct comparison with Figure 2. The same experimental conditions as those reported in the caption of Figure 2. The inset on the right in Figure 5 shows the comparison of the voltametric traces with Fe(beacen)Cl in the presence of proton donors (blue traces) with the one registered in the absence of proton donors (black trace, see also Figure 2), that allows one to appreciate the current enhancement of the first catalytic process in the presence of proton donors; see previous discussion. In the presence of the proton donors, variation of the $E_{1/2}$ of the $Fe^{III/II}$ couple and cathodic $Fe^{III} \rightarrow Fe^{II}$ wave splitting are observed, see Figures S12 and S13 and Table S1. These observations are coherent with protonation equilibria of the complex, presumably at the ligand phenoxide and/or enolate oxygen sites, along with PhOH or TFE coordination to Fe^{III} with competition with the Cl^- ligand for apical coordination see refs [11,12].

Table 2. Electrochemical reduction of CO_2 with iron complexes in the presence of phenol (PhOH) or trifluoroethanol (TFE) proton donors.

Iron Complex	Proton Donor	E_p (V vs. Fc^+/Fc)	$-i_{CO2}/i_{N2}$ [a]	FY, CO (FY, H_2) [b]	CO vs. H_2 Selectivity [b,c]
Fe(salophen)Cl [12]	PhOH 0.5 M [11]	−1.99	−4.3	50 (1)	98
Fe(salen)Cl	PhOH 0.5 M	−2.25	−7.6	40 (<0.5)	>98 [d]
	TFE 0.3 M	−2.29	−5.0	21 (<0.1)	>99 [e]
Fe(acacen)Cl	PhOH 0.5 M	−2.31	−9.7 [f]	5.5 (13.7)	28
	TFE 0.3 M	−2.31	−10.0	13.5 (0.55)	96
Fe(beacen)Cl	PhOH 0.5 M	−2.18	−10.0	10 (14.4)	41
	TFE 0.3 M	−2.15	−7.8	42 (<0.1)	>99
Fe(acacsalen)Cl	PhOH 0.5 M	−2.19	−7.4	<1 (14.8)	<1
	TFE 0.3 M	−2.31	−5.8	18 (6.6)	73

[a] Determined from CV traces; i_{CO2} is the cathodic peak current in the presence of CO_2 and of the proton donor; i_{N2} is the cathodic peak current of the $Fe^{II/I}$ couple under dinitrogen. [b] Determined after two electrons passed per iron center. [c] CO vs. H_2 selectivity, defined as mol(CO)/{mol(CO)+mol(H_2)}, and determined after two electrons passed per Iron center. [d] A selectivity >98% was maintained up to 25 electrons passed per iron center, with 4 turnovers for CO production. [e] A selectivity >99% was maintained up to 20 electrons passed per iron center, with 2.6 turnovers for CO production. [f] Ill-defined peak, due to the underlying current associated with the discharge of PhOH reduction.

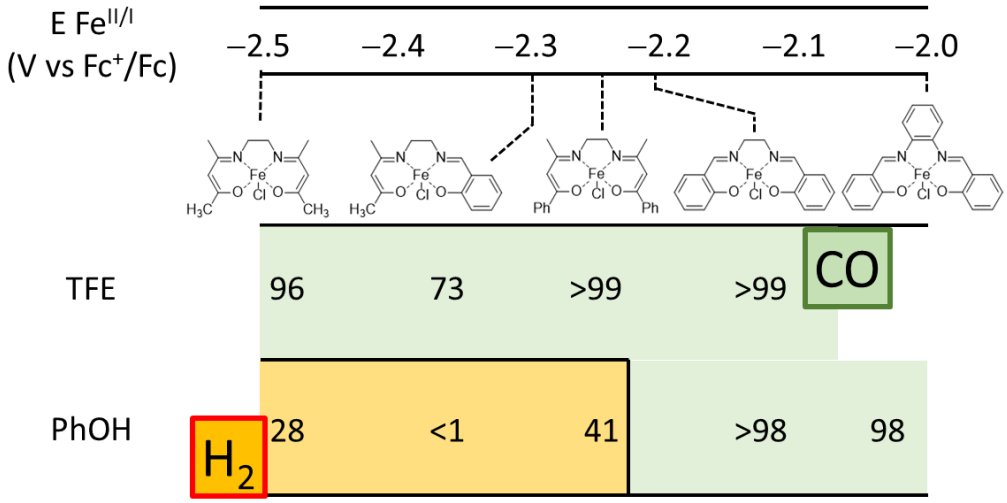

Figure 6. CO vs. H_2 selectivity in CPE experiments with Iron complexes, depending on the proton donor. The selectivity was compared after the same charged passed, in particular at two electrons per iron catalyst (see Table 2), and used as performance indicators in the series.

4. Discussion

From a catalytic perspective, Fe(salen)Cl appears the most promising candidate in the reduction of CO_2. Fe(salen)Cl allowed the maintenance of a selectivity >98% along with electrolysis after 25 and 20 electrons passed per Iron center with PhOH and TFE, respectively, reaching a turnover number for CO production of 4.6 and 2.6 with PhOH and TFE, respectively. Although still limited, the TON values confirm the possibility for Fe(salen) to operate catalytically. For the sake of comparison, a TON of 8 and a Faradaic yield of 48% for CO were found under electrochemical conditions for one of the most recently investigated catalyst for reduction of CO_2 to CO, i.e., Fe(qpy) (qpy = 2,2′:6′,2″:6″,2‴-quaterpyridine) [5,6]. Three TONs were registered for Fe(salophen) with PhOH [12]. The slightly higher stability of Fe(salen) with respect to Fe(salophen) could be associated with the more negative potential required for the reduction of the imine bond [32], which can be the origin of demetalation, responsible for the nucleation of Fe clusters [33] and the electrodeposition of Fe(0) nanoparticles [12,26,34]. CO_2 reduction

occurring through a molecular pathway is supported by the lack of any activity of the working electrode at the end of the CPE experiments. Indeed, the working electrode used in "unpolished tests" (i.e., CPE experiments in which the initial surface state of the working electrode was not restored run in electrolyte solutions without the catalyst, ref [26], pass only a limited amount of charge, displaying negligible activity towards proton reduction and no activity towards CO_2 reduction. Eventual deposition of electroactive iron particles on the carbon electrode would instead produce an electrode prone to enhanced H_2 evolution in the presence of proton donors, refs [12,34]. It is also worth to mention that in this latter case CO_2 reduction to CH_4 could reasonably be observed, with FE values in the 1–3% range, see refs [12,34]. A subsequent electrolysis on a Fe(salen) solution previously employed (25 electrons passed per iron centre, with phenol proton donor) displayed a lower current (<10% with respect to the first electrolysis) and negligible activity toward CO_2 reduction. These results are coherent with Fe(salen) Faradaic decomposition side-processes to inert species. The robustness of the imine bond and the stabilization of the reduced Fe^I intermediate are thus the main target to improve operative stability. It is also worth mentioning that catalyst stability is extremely dependent on operative conditions (i.e., electrochemical or photochemical, see refs. [5,6]). In some cases, heterogenization of molecular catalysts was also shown to lead to improvements in stability.

Benchmarking of Fe(salen)Cl should also consider overpotential (η) and the rate constant (k_{cat}), whose estimation can be directly determined by the CV analysis [35]. η was determined from the difference between the peak potential of the catalytic wave and the standard reduction potential associated with the CO_2/CO evaluated in the same conditions (E^0 (CO_2/CO) = −1.34 vs. Fc^+/Fc) [12,29]: In the presence of 0.5 M phenol, η results in 0.91 V, which is significantly higher than the one observed for Fe(salophen) under similar conditions, η = 0.65 V, due to the increased electron-donating character of the salen ligand that requires a more negative potential to generate the Fe^I species. Concerning k_{cat}, given the impossibility of reaching an "S-shaped" wave typical of pure kinetic conditions even operating at high scan rates (up to 16 Vs^{-1}), foot-of-the-wave analysis (FOWA) was conducted on the cyclic voltammetry (see treatment in Supplementary Information, and Figure S17), providing an estimation of k_{cat} 5×10^4 s^{-1} (under the same conditions, Fe(salophen) exhibited 1×10^3 s^{-1}) [12]. These key performance indicators are summarized in the Catalytic Tafel plot (Figure S18).

A final point of discussion deals with the initial CO vs. H_2 selectivity observed in CPE experiments. The selectivity for CO of Fe(salen) was supported by the persistence of the spectroscopic features of the Fe^I intermediate along with SEC-UV/Vis experiments in the presence of both proton donors employed (Figure 7). This supports the limited reactivity of Fe^I(salen) with PhOH and TFE, thus favoring its reactivity with CO_2 and supporting the observed CO_2-to-CO reaction pathway (Table 2 and Figure 6). Further evidence is provided by the CV traces of Fe(salen)Cl in the presence of PhOH and TFE, where no current discharges attributable to H_2 production at the level of the $Fe^{II/I}$ couple are observed (Figures S10 and S11).

Conversely, for Fe(acacen)Cl, Fe(beacen(Cl), and Fe(acacsalen)Cl, the nature of the proton donor has an impact on the observed products [27], and in particular on the initial CO vs. H_2 selectivity (Figure 6). While the use of TFE favors CO formation (selectivity 96, >99, and 73% for Fe(acacen)Cl, Fe(beacen(Cl), and Fe(acacsalen)Cl, respectively), the presence of phenol switches the process towards H_2 production in the early stage of the experiment (associated with a drop in CO vs. H_2 selectivity: 28, 41, <1% for Fe(acacen)Cl, Fe(beacen(Cl), and Fe(acacsalen)Cl, respectively, see Table 2). These results suggest direct reactivity of electrogenerated Fe^I species in this series with phenol, as confirmed by CV (rise in the cathodic current at the level of the $Fe^{II/I}$ couple in the presence of phenol under N_2 atmosphere, Figure S10) and by SEC-UV/Vis experiments. Indeed, the electrogeneration of the Fe^I intermediate under N_2 atmosphere in the presence of phenol for Fe(beacen)Cl is a representative case (Figure S19), the diagnostic feature of Fe^I species is significantly abated, while new absorptions rise in the 400–800 nm region. Conversely, in the presence

of TFE, a similar spectroscopic outcome with respect to the one previously discussed in the absence of proton donors is observed (rising of the MLCT band at 340 nm, see Figure 4 and related discussion).

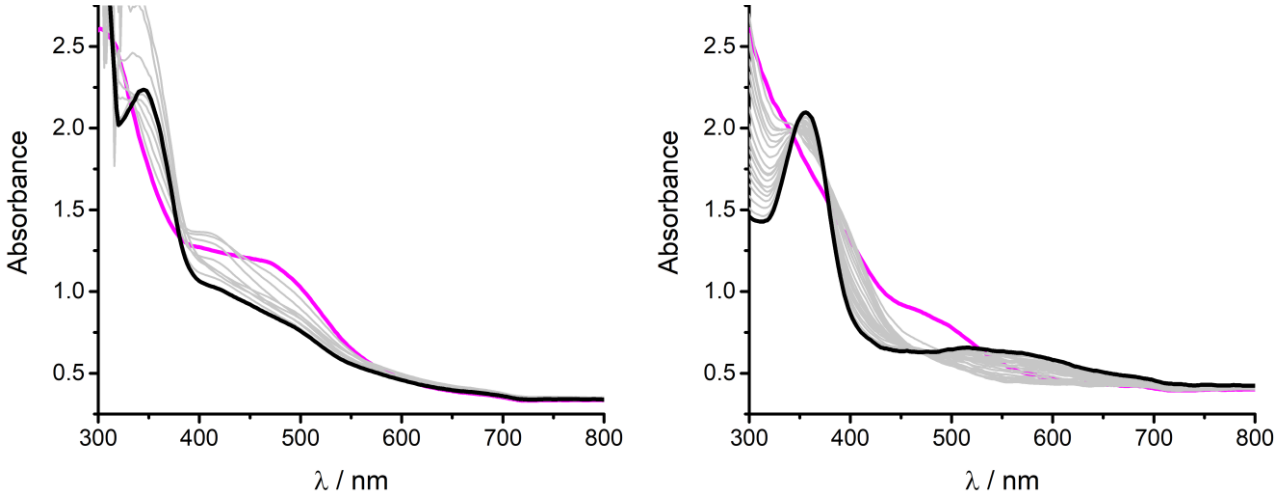

Figure 7. SEC-UV/Vis traces of Fe(salen)Cl under N_2 atmosphere in the presence of 0.5 M PhOH (**left**) and 0.3 M TFE (**right**) proton donors, at the potentials corresponding to the generation of the formal Fe^I state (−2.21 V vs. Fc^+/Fc).

The reactivity of Fe^I(beacen) with phenol can potentially involve both the iron center and the ligand. The H_2 evolution observed for the β-diketyl-derived complexes in the presence of phenol could possibly be associated with the formation of iron hydride intermediates [11], and their further reaction with a second phenol equivalent; metal hydrides with sufficient hydricity [36] could also be responsible for formate production [37] (not detected in this study). Iron hydride generation might also be assisted by the previous protonation of the methine site, ultimately producing a hydride-transfer relay in the ligand scaffold [38]. Indeed, protonation of the imine group or of the methine carbon in β position to the imine and enolate can be considered under cathodic conditions [11,19], and both processes could account for the Faradaic decomposition of the catalysts; the presence of the methine group seems likely responsible for the faster complex degradation under electrolysis conditions for Fe(beacen), Fe(acacen), and Fe(acacsalen), regardless of the proton donor nature (the current drops after three electrons passed per iron center (Figure S15) and marked UV/Vis change (Figure S16)).

5. Conclusions

We have reported an electrochemical investigation of four $Fe^{III}(L_{N2O2})Cl$ complexes (L_{N2O2} is a tetradentate N_2O_2 Schiff base ligand), and their potential application in the reduction of carbon dioxide. The main results can be summarized as follows:

(i) The $Fe^{III}(L_{N2O2})Cl$ complexes display two metal-based reductions, involving $Fe^{III/II}$ and $Fe^{II/I}$ couples; the potential associated with the $Fe^{II/I}$ couple, relevant to reactivity with CO_2, correlates with the electronic character of the L_{N2O2} (in terms of the energy of the highest occupied σ-donating orbital) and with the energy of the metal-to-ligand charge transfer absorption of the Fe^I intermediate, determined by SEC-UV/Vis.

(ii) The Fe^I intermediates react with CO_2, as proven by CV and SEC-UV/Vis investigation.

(iii) For Fe(salen)Cl, in the presence of phenol or trifluoroethanol proton donors, the process is associated with the selective reduction of CO_2 to CO (no H_2 and formate are detected along with the electrolysis); in the presence of 0.5 M phenol, key performance indicators are an overpotential of 0.91 V, a catalytic rate constant of 5×10^4 s^{-1}, and a turnover number of 4. CO_2 reduction occurs through a homogeneous route, and the transformation of Fe(Salen) into an electrochemically inert species occurs.

(iv) In the case of Fe(acacen)Cl, Fe(beacen(Cl), and Fe(acacsalen)Cl, the production of CO is observed only with TFE proton donor, while phenol leads to the evolution of H_2 from the early stage of electrolysis. In all cases, the electrolysis current drops suddenly after three electrons passed per iron center, indicating a higher instability of these species, likely associated with the protonation under cathodic conditions of the ketylacetoneimine pendant of the ligands.

The structure/reactivity correlations involving active low-valent Fe intermediates and the indications on the selectivity and stability of the coordination complexes under cathodic conditions and depending on the proton donor nature can be valuable in the design of more efficient and more robust catalysts.

Supplementary Materials: The following are available online at https://www.mdpi.com/article/10.3390/en14185723/s1, including detailed experimental procedures and supplementary Figures S1–S19 cited in the main text.

Author Contributions: Conceptualization, R.B. and A.S.; methodology, R.B., D.C., F.C. and A.S.; formal analysis, R.B., D.C., F.C. and A.S.; investigation, R.B., D.C. and F.C.; writing, R.B. and A.S.; supervision, A.S.; project administration, A.S.; funding acquisition, A.S. All authors have read and agreed to the published version of the manuscript.

Funding: This research was funded by Fondazione Cassa di Risparmio Padova e Rovigo (CaRiPaRo), grant Synergy within the call Ricerca Scientifica di Eccellenza 2018.

Institutional Review Board Statement: Not applicable.

Informed Consent Statement: Not applicable.

Data Availability Statement: Data is contained within the article or Supplementary Material.

Acknowledgments: We thank Mauro Meneghetti and Stefano Mercanzin for the invaluable support in the construction of the gas-tight electrolysis cell and for technical support, and Loris Calore for the prompt support for elemental analysis of the compounds.

Conflicts of Interest: The authors declare no conflict of interest.

References

1. De Oliveira, F.T.; Chanda, A.; Banerjee, D.; Shan, X.; Mondal, S.; Que, L.; Bominaar, E.L.; Münck, E.; Collins, T.J. Chemical and spectroscopic evidence for an Fe^{V}-oxo complex. *Science* **2007**, *315*, 835–838. [CrossRef] [PubMed]
2. Bell, S.R.; Groves, J.T. A highly reactive P450 model compound I. *J. Am. Chem. Soc.* **2009**, *131*, 9640–9641. [CrossRef] [PubMed]
3. Bhugun, I.; Lexa, D.; Savéant, J.M. Catalysis of the electrochemical reduction of carbon dioxide by iron(0) porphyrins: Synergystic effect of weak Brönsted acids. *J. Am. Chem. Soc.* **1996**, *118*, 1769–1776. [CrossRef]
4. Chalkley, M.J.; Drover, M.W.; Peters, J.C. Catalytic N_2-to-NH_3 (or -N_2H_4) Conversion by Well-Defined Molecular Coordination Complexes. *Chem. Rev.* **2020**, *120*, 5582–5636. [CrossRef]
5. Cometto, C.; Chen, L.; Lo, P.K.; Guo, Z.; Lau, K.C.; Anxolabéhère-Mallart, E.; Fave, C.; Lau, T.C.; Robert, M. Highly Selective Molecular Catalysts for the CO_2-to-CO Electrochemical Conversion at Very Low Overpotential. Contrasting Fe vs. Co Quaterpyridine Complexes upon Mechanistic Studies. *ACS Catal.* **2018**, *8*, 3411–3417. [CrossRef]
6. Guo, Z.; Cheng, S.; Cometto, C.; Anxolabéhère-Mallart, E.; Ng, S.-M.; Ko, C.-C.; Lu, G.; Chen, L.; Robert, M.; Lau, T.-C. Highly Efficient and Selective Photocatalytic CO_2 Reduction by Iron and Cobalt Quaterpyridine Complexes. *J. Am. Chem. Soc.* **2016**, *138*, 9413–9416. [CrossRef] [PubMed]
7. Bhunia, S.; Rana, A.; Hematian, S.; Karlin, K.D.; Dey, A. Proton Relay in Iron Porphyrins for Hydrogen Evolution Reaction. *Inorg. Chem.* **2021**. [CrossRef]
8. Bonetto, R.; Crisanti, F.; Sartorel, A. Carbon Dioxide Reduction Mediated by Iron Catalysts: Mechanism and Intermediates That Guide Selectivity. *ACS Omega* **2020**, *5*, 21309–21319. [CrossRef] [PubMed]
9. Costentin, C.; Robert, M.; Savéant, J.M. Current Issues in Molecular Catalysis Illustrated by Iron Porphyrins as Catalysts of the CO_2-to-CO Electrochemical Conversion. *Acc. Chem. Res.* **2015**, *48*, 2996–3006. [CrossRef]
10. Pun, S.N.; Chung, W.H.; Lam, K.M.; Guo, P.; Chan, P.H.; Wong, K.Y.; Che, C.M.; Chen, T.Y.; Peng, S.M. Iron(I) complexes of 2,9-bis(2-hydroxyphenyl)-1,10-phenanthroline (H_2dophen) as electrocatalysts for carbon dioxide reduction. X-ray crystal structures of $[Fe(dophen)Cl]_2{\cdot}2HCON(CH_3)_2$ and $[Fe(dophen)(N\text{-}MeIm)_2]ClO_4$ (N-MeIm = 1-methylimidazole). *J. Chem. Soc. Dalt. Trans.* **2002**, 575–583. [CrossRef]

11. Nichols, A.W.; Chatterjee, S.; Sabat, M.; MacHan, C.W. Electrocatalytic Reduction of CO_2 to Formate by an Iron Schiff Base Complex. *Inorg. Chem.* **2018**, *57*, 2111–2121. [CrossRef]
12. Bonetto, R.; Altieri, R.; Tagliapietra, M.; Barbon, A.; Bonchio, M.; Robert, M.; Sartorel, A. Electrochemical Conversion of CO_2 to CO by a Competent Fe^I Intermediate Bearing a Schiff Base Ligand. *ChemSusChem* **2020**, *13*, 4111–4120. [CrossRef] [PubMed]
13. Nishida, Y.; Oshio, S.; Kida, S. Synthesis and Magnetic properties of Iron(III) complexes with several quadridentate Schiff bases. *Bull. Chem. Soc. Jpn.* **1977**, *50*, 119–122. [CrossRef]
14. Cisterna, J.; Artigas, V.; Fuentealba, M.; Hamon, P.; Manzur, C.; Hamon, J.R.; Carrillo, D. Pentacoordinated chloro-iron(III) complexes with unsymmetrically substituted N_2O_2 quadridentate schiff-base ligands: Syntheses, structures, magnetic and redox properties. *Inorganics* **2018**, *6*, 5. [CrossRef]
15. Liang, Y.; Duan, R.L.; Hu, C.Y.; Li, L.L.; Pang, X.; Zhang, W.X.; Chen, X.S. Salen-iron complexes: Synthesis, characterization and their reactivity with lactide. *Chinese J. Polym. Sci.* **2018**, *36*, 185–189. [CrossRef]
16. Cozzolino, M.; Leo, V.; Tedesco, C.; Mazzeo, M.; Lamberti, M. Salen, salan and salalen iron(III) complexes as catalysts for CO_2/epoxide reactions and ROP of cyclic esters. *Dalt. Trans.* **2018**, *47*, 13229–13238. [CrossRef]
17. Wang, X.; Pennington, W.T.; Ankers, D.L.; Fanning, J.C. Comparative crystal structure examination of some iron(III) quadridentate schiff base complexes. *Polyhedron* **1992**, *11*, 2253–2264. [CrossRef]
18. Böttcher, A.; Takeuchi, T.; Hardcastle, K.I.; Meade, T.J.; Gray, H.B.; Cwikel, D.; Kapon, M.; Dori, Z. Spectroscopy and Electrochemistry of Cobalt(III) Schiff Base Complexes. *Inorg. Chem.* **1997**, *36*, 2498–2504. [CrossRef]
19. Isse, A.A.; Gennaro, A.; Vianello, E. Electrochemical reduction of Schiff base ligands H_2salen and H_2salophen. *Electrochim. Acta* **1997**, *42*, 2065–2071. [CrossRef]
20. Chirik, P.J.; Wieghardt, K. Radical ligands confer nobility on base-metal catalysts. *Science* **2010**, *327*, 794–795. [CrossRef] [PubMed]
21. Udugala-Ganehenege, M.Y.; Dissanayake, N.M.; Liu, Y.; Bond, A.M.; Zhang, J. Electrochemistry of nickel(II) and copper(II) N,N′-ethylenebis(acetylacetoniminato) complexes and their electrocatalytic activity for reduction of carbon dioxide and carboxylic acid protons. *Transit. Met. Chem.* **2014**, *39*, 819–830. [CrossRef]
22. Ueda, T.; Inazuma, N.; Komatsu, D.; Yasuzawa, H.; Onda, A.; Guo, S.X.; Bond, A.M. Comparison of chemical interactions with Li^+ and catalytic reactivity of electrochemically generated $[Fe^ICl(L)]^{2-}$ and $[Co^I(L)]^-$ complexes (L = salen or salophen). *Dalt. Trans.* **2013**, *42*, 11146–11154. [CrossRef] [PubMed]
23. Costes, J.P.; Tommasino, J.B.; Carré, B.; Soulet, F.; Fabre, P.L. Electrochemical studies of iron(III) Schiff base complexes-II. Dimeric μ-oxo $[Fe^{III}(N_2O_2)]_2O$ complexes. *Polyhedron* **1995**, *14*, 771–780. [CrossRef]
24. Matosziuk, L.M.; Holbrook, R.J.; Manus, L.M.; Heffern, M.C.; Ratner, M.A.; Meade, T.J. Rational design of $[Co(acacen)L_2]$+ inhibitors of protein function. *J. Chem. Soc. Dalt. Trans.* **2013**, *42*, 4002–4012. [CrossRef] [PubMed]
25. Cini, R.; Cinquantini, A.; Orioli, P.L.; Mealli, C.; Sabat, M. The effect of d electron configuration on a mononuclear transition metal species of a Schiff-base ligand with a N_2S_2 donor set (sacacen). *Can. J. Chem.* **1984**, *62*, 2908–2913. [CrossRef]
26. Lee, K.J.; McCarthy, B.D.; Dempsey, J.L. On decomposition, degradation, and voltammetric deviation: The electrochemist's field guide to identifying precatalyst transformation. *Chem. Soc. Rev.* **2019**, *48*, 2927–2945. [CrossRef]
27. Ngo, K.T.; McKinnon, M.; Mahanti, B.; Narayanan, R.; Grills, D.C.; Ertem, M.Z.; Rochford, J. Turning on the Protonation-First Pathway for Electrocatalytic CO_2 Reduction by Manganese Bipyridyl Tricarbonyl Complexes. *J. Am. Chem. Soc.* **2017**, *139*, 2604–2618. [CrossRef] [PubMed]
28. Costentin, C.; Drouet, S.; Robert, M.; Savéant, J.-M. A Local Proton Source Enhances CO_2 Electroreduction to CO by a Molecular Fe Catalyst. *Science* **2012**, *338*, 90–94. [CrossRef]
29. Azcarate, I.; Costentin, C.; Robert, M.; Savéant, J.M. Through-Space Charge Interaction Substituent Effects in Molecular Catalysis Leading to the Design of the Most Efficient Catalyst of CO_2-to-CO Electrochemical Conversion. *J. Am. Chem. Soc.* **2016**, *138*, 16639–16644. [CrossRef]
30. Lam, Y.C.; Nielsen, R.J.; Gray, H.B.; Goddard, W.A. A Mn Bipyrimidine Catalyst Predicted to Reduce CO_2 at Lower Overpotential. *ACS Catal.* **2015**, *5*, 2521–2528. [CrossRef]
31. Queyriaux, N.; Abel, K.; Fize, J.; Pécaut, J.; Orio, M.; Hammarström, L. From non-innocent to guilty: On the role of redox-active ligands in the electro-assisted reduction of CO_2 mediated by a cobalt(II)-polypyridyl complex. *Sustain. Energy Fuels* **2020**, *4*, 3668–3676. [CrossRef]
32. Isse, A.A.; Gennaro, A.; Vianello, E.; Floriani, C. Electrochemical reduction of carbon dioxide catalyzed by $[Co^I$(salophen)Li]. *J. Mol. Catal.* **1991**, *70*, 197–208. [CrossRef]
33. Toniolo, D.; Scopelliti, R.; Zivkovic, I.; Mazzanti, M. Assembly of High-Spin $[Fe_3]$ Clusters by Ligand-Based Multielectron Reduction. *J. Am. Chem. Soc.* **2020**, *142*, 7301–7305. [CrossRef] [PubMed]
34. Cometto, C.; Chen, L.; Mendoza, D.; Lassalle-Kaiser, B.; Lau, T.C.; Robert, M. An Iron Quaterpyridine Complex as Precursor for the Electrocatalytic Reduction of CO_2 to Methane. *ChemSusChem* **2019**, *12*, 4500–4505. [CrossRef] [PubMed]
35. Costentin, C.; Drouet, S.; Robert, M.; Savéant, J.M. Turnover numbers, turnover frequencies, and overpotential in molecular catalysis of electrochemical reactions. Cyclic voltammetry and preparative-scale electrolysis. *J. Am. Chem. Soc.* **2012**, *134*, 11235–11242. [CrossRef]

36. Waldie, K.M.; Ostericher, A.L.; Reineke, M.H.; Sasayama, A.F.; Kubiak, C.P. Hydricity of Transition-Metal Hydrides: Thermodynamic Considerations for CO_2 Reduction. *ACS Catal.* **2018**, *8*, 1313–1324. [CrossRef]
37. Loewen, N.D.; Neelakantan, T.V.; Berben, L.A. Renewable Formate from C-H Bond Formation with CO_2: Using Iron Carbonyl Clusters as Electrocatalysts. *Acc. Chem. Res.* **2017**, *50*, 2362–2370. [CrossRef] [PubMed]
38. Solis, B.H.; Maher, A.G.; Honda, T.; Powers, D.C.; Nocera, D.G.; Hammes-Schiffer, S. Theoretical analysis of cobalt hangman porphyrins: Ligand dearomatization and mechanistic implications for hydrogen evolution. *ACS Catal.* **2014**, *4*, 4516–4526. [CrossRef]